pre print in 2013 European journal of control

Selective Model Inversion and Adaptive Disturbance Observer for Time-varying Vibration Rejection on an Active-Suspension Benchmark

Xu Chen and Masayoshi Tomizuka

***Abstract*—This paper presents an adaptive control scheme for identifying and rejecting unknown and/or time-varying narrow-band vibrations. We discuss an idea of safely and adaptively inverting a (possibly non-minimum phase) plant dynamics at selected frequency regions, so that structured disturbances (especially vibrations) can be estimated and canceled from the control perspective. By taking advantage of the disturbance model in the design of special infinite-impulse-response (IIR) filters, we can reduce the adaptation to identify the minimum amount of parameters, achieve accurate parameter estimation under noisy environments, and flexibly reject the narrow-band disturbances with clear tuning intuitions. Evaluation of the algorithm is performed via simulation and experiments on an active-suspension benchmark.**

***Index Terms*—adaptive regulation, loop shaping, inverse control, vibration rejection, active suspension**

I. Introduction

The rejection of single and multiple narrow-band disturbances is a fundamental problem in many mechanical systems that involve periodic motions. For example, the shaking mechanism in active suspensions [1], the rotating disks in hard disk drives [2], and the cooling fans for computer products [3], all generate vibrations that are composed of sinusoidal components in nature. Challenges of the problem are that we often do not have accurate knowledge of the disturbance frequencies, and that in many applications the disturbance characteristics may even change w.r.t. time and/or among different products (e.g., in the hard disk drive industry [4]).

In various situations, hardware limitations or excessive cost make it infeasible to re-design the hardware for reducing these disturbances, and it is only possible to address the problem from the control-engineering approach. As narrow-band disturbances are composed of sinusoidal signal components, controllers can be customized to incorporate the disturbance structure to asymptotically reject the vibrations. This internal-model-principle [5] based perspective has been investigated in feedback control algorithms in [1], [3], [6]–[8], among which [6], [7] used state-space designs, and [1], [3], [8] applied Youla Parameterization, a.k.a. all stabilizing controllers, with a Finite Impulse Response (FIR) adaptive Q filter. Alternatively, the disturbance frequency can be firstly estimated and then applied for controller design. This indirect-adaptive-control perspective has been considered in [9]–[11]. Indeed, frequency identification of narrow-band signals is a problem that receives great research attention itself. Among the related literature we can find: (i) methods using nonparametric spectrum estimation or eigen analysis (subspace methods) [12], [13]; (ii) online adaptive identification approaches [14]–[20]. Spectrum estimation and eigen analysis in general require more expensive computation within the sampling interval, and have lower resolutions for non-stationary processes. Among references in group (ii), for the identification of n frequency components, adaptive notch filters in the orders of $5n-1$ [19], $2n+6$ [20], $3n$ [15]–[17], and $2n$ [14], have been discussed.

In this paper we discuss a new adaptive incorporation of the internal model principle for asymptotic rejection of narrow-band disturbances. Different from the FIR-based adaptive algorithms, we construct the controllers and adaptation with Infinite Impulse Response (IIR) filters and inverse system models. Applying these considerations we are able to obtain a structured controller parameterization that requires the minimum number of adaptation parameters. An additional consideration is that adaptation on IIR structures enables direct adaptive control with adaptation algorithms that use the parallel predictor, which is essential for accurate parameter convergence under noisy environments [21]. The importance of this aspect can also be seen from the aforementioned literature on frequency identification. Finally, with the inverse-model based design, the internal signals in the proposed algorithm have clear physical meanings. The controller structure extends the idea in [2]. The main results of this paper, i.e., the design of inverse models, the derivation of the cascaded IIR filters, and the adaptation algorithm for time-varying disturbance rejection, however, are all newly developed. An additional contribution is the application to a new class of systems that has characteristics quite different from the hard disk drive in [2]. A short version of the paper appeared in [22]. This article is a substantially modified version with proofs and derivations of equations, extended analysis of the algorithms (especially the adaptive-control part), and implementation details as well as the full simulation and experimental results.

The algorithm is evaluated on an active suspension system that has been described in [23]. Fig. 1 presents the frequency response of the plant. It can be observed that the system has a group of resonant and anti-resonant

X. Chen and M. Tomizuka are with the Department of Mechanical Engineering, University of California, Berkeley, CA, 94720, USA (email: maxchen@me.berkeley.edu; tomizuka@me.berkeley.edu)

modes, especially at around 50 Hz and 100 Hz. Additionally, the system is open-loop stable but has multiple lightly damped mid-frequency zeros and high-frequency nonminimum-phase zeros. These characteristics place additional challenges not just for adaptive disturbance rejection, but also for general feedback control [24].

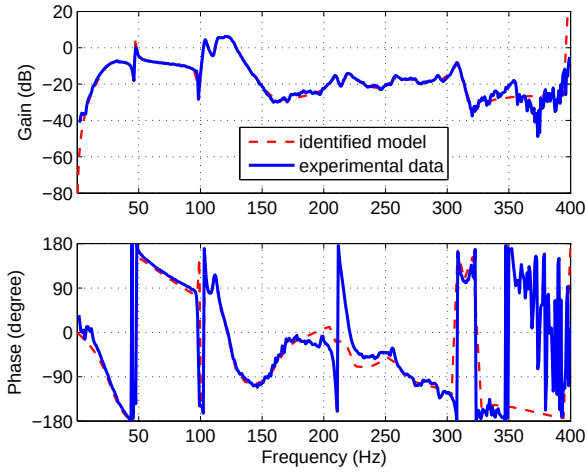

Figure 1: Frequency response of the plant

II. Selective Model Inversion

Fig. 2 shows the proposed control scheme. We have the following relevant signals and transfer functions:

- $P(z^{-1})$ and $\hat{P}(z^{-1})$: the plant and its identified model. They are open-loop stable in the benchmark;
- $C(z^{-1})$: the baseline controller designed to provide a robustly stable closed loop. For controlling a stable plant, we assume that $C(z^{-1})$ is also stable;
- $d(k)$ and $\hat{d}(k)$: the actual (unmeasurable) disturbance and its online estimate. To see this, note that

$$\hat{d}(k) = P(q^{-1})u(k) + d(k) - \hat{P}(q^{-1})u(k) \approx d(k),$$

where q^{-1} is the one-step-delay operator (in this paper, $P(z^{-1})$, $P(q^{-1})$, and $P(e^{-j\omega})$ are used to denote respectively the transfer function, the pulse transfer function, and the frequency response of $P(z^{-1})$). $\hat{d}(k)$ is quite accurate as $\hat{P}(z^{-1})$ is identified quite accurately in the benchmark. The minimum requirement for $\hat{P}(z^{-1})$ is that is should be accurate within the frequency region where disturbance occurs. The noise due to model mismatch, if any, can be later reduced by filtering in the adaptation scheme;

- $y(k)$: the measured residual errors;
- $P_m^{-1}(z^{-1})$ and z^{-m}: these are constructed such that:

1) $P_m(z^{-1})$ has a relative degree of zero (and hence $P_m^{-1}(z^{-1})$ is realizable);

2) $P_m^{-1}(z^{-1})$ is stable; and

3) within the frequency range of the possible disturbances, $P(z^{-1})\big|_{z=e^{j\omega}} \approx z^{-m}P_m(z^{-1})\big|_{z=e^{j\omega}}$, namely, $P_m^{-1}(z^{-1})$ is a nominal inverse model (without delays) of $P(z^{-1})$. Indeed in Fig. 1, the dashed line depicts the frequency response of $z^{-m}P_m(z^{-1})$, which matches well with the experimental frequency response up to around 350 Hz;

- Parameter adaptation algorithm: provides online information of the characteristics of $\hat{d}(k)$;
- $c(k)$: the compensation signal to asymptotically reject the narrow-band disturbance in $d(k)$.

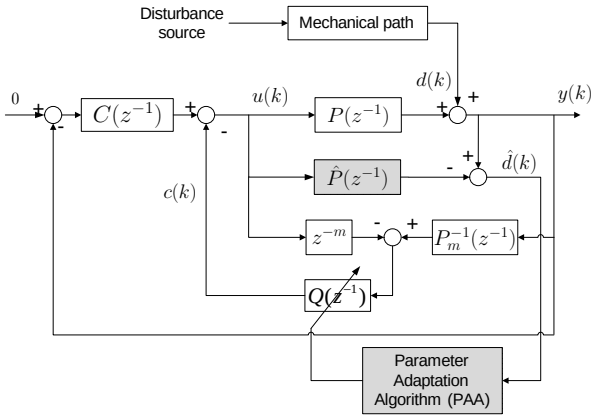

Figure 2: Structure of the proposed control scheme

Ignoring first the shaded blocks (about parameter adaptation) in Fig. 2, we have

$$\begin{aligned} y(k) &= d(k) + P(q^{-1})u(k) \\ u(k) &= -C(q^{-1})y(k) - c(k) \\ c(k) &= Q(q^{-1})[P_m^{-1}(q^{-1})y(k) - q^{-m}u(k)] \end{aligned}$$

from which we can derive the sensitivity function, namely, the transfer function from $d(k)$ to $y(k)$:

$$S(z^{-1}) = G_{d2y}(z^{-1}) = \left(1 - z^{-m}Q(z^{-1})\right)/X(z^{-1}) \quad (1)$$

$$X(z^{-1}) = 1 + P(z^{-1})C(z^{-1}) + Q(z^{-1})(P_m^{-1}(z^{-1})P(z^{-1}) - z^{-m}) \quad (2)$$

From the frequency-response perspective (replace z^{-1} with $e^{-j\omega}$), if $P(e^{-j\omega}) = e^{-jm\omega}P_m(e^{-j\omega})$ in (1) and (2), then the last term in $X(e^{-j\omega})$ vanishes and

$$S(e^{-j\omega}) = \left(1 - e^{-jm\omega}Q(e^{-j\omega})\right)/\left(1 + P(e^{-j\omega})C(e^{-j\omega})\right). \quad (3)$$

If we design a Q-filter $Q(z^{-1})$ with its frequency response as shown in Fig. 3, then $1 - e^{-mj\omega}Q(e^{-j\omega})$, and thus $G_{d2y}(e^{-j\omega})$ in (1), will become zero at the center frequencies of $Q(z^{-1})$, namely, disturbances occurring at these frequencies will be strongly attenuated. Assume first that vibrations occur exactly at 60 Hz and 90 Hz. $Q(z^{-1})$ will filter out all other frequency components such that its output $c(k)$ consists of signals only at the disturbance frequencies. More specifically, $c(k)$ is actually an estimated version of $P^{-1}(q^{-1})d(k)$ if $d(k)$ contains just narrow-band vibrations. To see this, notice in Fig. 2, that the control signal $u(k)$ flows through two paths to reach the summing junction before $Q(z^{-1})$: one from the plant $P(z^{-1})$ to the inverse $P_m^{-1}(z^{-1})$, and the other through z^{-m}. Hence the effect of $u(k)$ gets canceled at the summing junction before $Q(z^{-1})$, and only the filtered disturbance $P_m^{-1}(q^{-1})d(k)$ enters $Q(z^{-1})$.

We remark that the shape of $Q(z^{-1})$ in Fig. 3 is central in the proposed design scheme. Uncertainties exist in

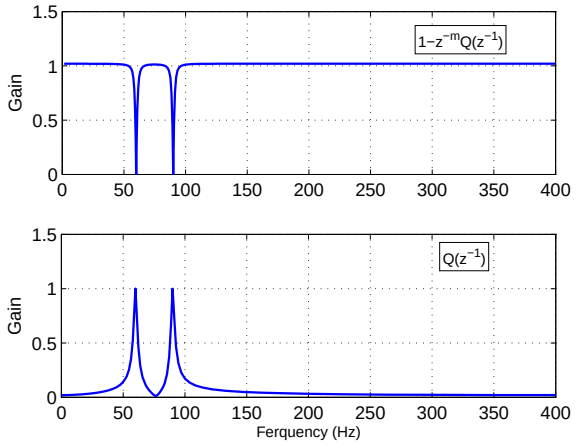

Figure 3: Frequency response of a Q-filter example

$P(z^{-1})$ (particularly at high frequencies), no matter how accurate $P_m(z^{-1})$ is constructed (based on modeling or system identification). It is not practical (and is even dangerous) to invert $P(z^{-1})$ over the entire frequency region. Keeping the magnitude of $Q(z^{-1})$ small except at the interested disturbance frequencies forms a "local/selective" model inverse (SMI) of the plant dynamics, such that errors due to model mismatches do not pass through $Q(z^{-1})$ and equation (3) remains a valid approximation of (1). In this way, closed-loop stability can be readily preserved since $1/(1+P(z^{-1})C(z^{-1}))$ is the sensitivity function of the baseline system (and hence is stable). A stable $Q(z^{-1})$ in this case will assure the stability of $S(z^{-1}) \approx (1-z^{-m}Q(z^{-1}))/(1+P(z^{-1})C(z^{-1}))$. Under the above conditions, the proposed scheme becomes a special form of Youla parameterization [25], where the add-on stable Q parameterization does not alter the closed-loop stability and focus on just disturbance cancellation. Of course, a prior assumption is that good model information can be obtained at the disturbance frequencies. If the system already has large uncertainties at the disturbance frequencies, it is best not to apply large control effort there in the first place.

The full stability result is summarized as follows:

Theorem 1. *Under the definitions listed at the beginning of this section, when there is no mismatch between $P(z^{-1})$ and $z^{-m}P_m(z^{-1})$, the closed loop in Fig. 2 is stable as long as $Q(z^{-1})$ is stable. When there is (stable and bounded) model uncertainty $\Delta(z^{-1})$ such that $P(z^{-1}) = z^{-m}P_m(z^{-1})[1+\Delta(z^{-1})]$, the closed loop is stable if $Q(z^{-1})$ is stable and*

$$\left|Q(e^{-j\omega})\right| < \left|\frac{1+P(e^{-j\omega})C(e^{-j\omega})}{\Delta(e^{-j\omega})}\right|, \ \forall \omega \in [0,\pi]. \qquad (4)$$

Proof: The nominal stability condition is a standard result of Youla parameterization. For robust stability, noting that $\Delta(z^{-1}) = P_m^{-1}(z^{-1})P(z^{-1}) - z^{-m}$, from (2), we can obtain the closed-loop characteristic polynomial:

$$1 + P(z^{-1})C(z^{-1}) + z^{-m}Q(z^{-1})\Delta(z^{-1}) = 0 \qquad (5)$$

The system is thus robustly stable if $\forall\ \omega \in [0,\pi]$

$$\left|e^{-jm\omega}\Delta(e^{-j\omega})Q(e^{-j\omega})\right| < \left|1+P(e^{-j\omega})C(e^{-j\omega})\right|. \qquad (6)$$

Noticing that the delay term $e^{-jm\omega}$ has unity magnitude, we can transform (6) to (4). ■

The benchmark system has visible uncertainties only at high frequencies (this is also the common case in general mechanical systems). (4) then provides very flexible design freedom for $Q(z^{-1})$. More important, the stability condition in Youla parameterization also holds when $Q(z^{-1})$ is made adaptive (but is still stable). This greatly benefits the rejection of unknown and time-varying vibrations when we update the parameters of $Q(z^{-1})$.

In the next section, we propose an approach to obtain the optimal inverse filter $P_m^{-1}(z^{-1})$. Following that, in Section IV we study the application of the internal model principle to design a customized $Q(z^{-1})$ that satisfies the frequency response in Fig. 3 for SMI.

III. Design of The Inverse Dynamics

In the aforementioned analysis we have assumed $P_m^{-1}(z^{-1})$ to be stable. It is well known that nonminimum-phase zeros in $P(z^{-1})$ not only make $P^{-1}(z^{-1})$ unstable but also cause control limitations. The benchmark system has multiple of such zeros. We discuss next an H_∞ treatment of the problem when designing $P_m^{-1}(z^{-1})$.

Let $\mathbf{S}$ denote the set of all stable discrete-time rational transfer functions. Recalling the ideal situation where $P(z^{-1}) = z^{-m}P_m(z^{-1})$, we search among $\mathbf{S}$ to find $M(z^{-1}) = P_m^{-1}(z^{-1})$ such that the following two criteria are satisfied:

(i) model matching: to minimize the cost function $\|W_1(z^{-1})\left(M(z^{-1})P(z^{-1}) - z^{-m}\right)\|_\infty$, namely, we minimize the maximum magnitude of the model mismatch $M(z^{-1})P(z^{-1}) - z^{-m}$, weighted by $W_1(z^{-1})$. The ideal solution, if $P^{-1}(z^{-1})$ is stable, is simply $M(z^{-1}) = z^{-m}P^{-1}(z^{-1})$. The weighting function determines the interested region where we would like to have good model accuracy.

(ii) gain constraint: as the inverse is used for processing the measured output signal, we should be careful not to amplify the noises in $y(k)$. Consider the problem of $\min\|W_2(z^{-1})M(z^{-1})P(z^{-1})\|_\infty$, where the magnitude of $M(z^{-1})P(z^{-1})$ is scaled by the weight $W_2(z^{-1})$. The optimal solution for this part alone would be that $M(z^{-1}) = 0$, i.e., $M(z^{-1})$ will not amplify any of its input components. To make full use of this gain constraint, we combine it with criterion (i) to form:

$$\min_{M(z^{-1})\in\mathbf{S}} \left\| \begin{bmatrix} W_1(z^{-1})\left(M(z^{-1})P(z^{-1}) - z^{-m}\right) \\ W_2(z^{-1})M(z^{-1})P(z^{-1}) \end{bmatrix} \right\|_\infty . \qquad (7)$$

The optimization in (7) finds the optimal inverse that preserves accurate model information in the frequency region specified by $W_1(z^{-1})$, and in the meantime penalizes excessive high gains of $M(z^{-1})$ at frequencies where $W_2(z^{-1})$ has high magnitudes. Typically $W_1(z^{-1})$ is a low-pass filter and $W_2(z^{-1})$ is a high-pass filter.

By the formulation of the problem, (7) falls into the framework of H_∞ control, and can be efficiently solved in the robust control toolbox in MATLAB. The solution exists as long as $P(z^{-1})$, $W_1(z^{-1})$, and $W_2(z^{-1})$ are stable. The order of $M(z^{-1})$ will be the sum of the orders of $W_1(z^{-1})$, $W_2(z^{-1})$, z^{-m} and $P(z^{-1})$. After solving (7), standard model reduction techniques can be applied to obtain a lower-order solution of $M(z^{-1})$. Actually, the dashed line in Fig. 1 is the resulted $z^{-m}P_m(z^{-1})$ where we have first obtained $P_m^{-1}(z^{-1})$ from (7) and then plotted the inverse of $P_m^{-1}(z^{-1})$ combined with z^{-m}. We can see that the optimal solution matches well with the actual plant dynamics, and moreover, $P_m^{-1}(z^{-1})$ is stable although $P(z^{-1})$ is nonminimum-phase.

Remark 1: similar to standard H_∞ controller design, the transfer function $P(z^{-1})$ is used in the proposed optimization. Hence the accuracy of $M(z^{-1})$ depends on the quality of $P(z^{-1})$. It is well understood that accurate modeling of very high-frequency dynamics is difficult, if possible at all, for all mechanical systems. Very sharp resonant or anti-resonant modes are also difficult to model exactly, since very small mismatch in the resonances (due to e.g. temperature change) will make $P(z^{-1})$ behave differently from the actual plant at the resonant frequencies. So practical design should avoid focusing on model inversion at very high frequencies, and be aware of the challenges in the presence of sharp resonances.

Remark 2: commonly, nonminimum-phase zeros occur at high frequencies. If there are such zeros in the frequency region of the vibrations, the problem becomes fundamentally much more challenging. For instance, if there is a pair of zeros at 150 Hz on the unit circle, then control input at 150 Hz will not be able to impact the output of the plant at all!

In the benchmark, to obtain the inverse model, we first apply system identification (we use the subspace system identification algorithm [26]) to obtain $P(z^{-1})$ from the collected input-output data, and then perform the algorithm in this section to get $P_m^{-1}(z^{-1})$. The order of the plant model (provided by the benchmark) for simulation is 25. The order of the obtained $P_m^{-1}(z^{-1})$, after standard model reduction, is 23. This value is quite reasonable considering the high-order nature of the physical system.

IV. Disturbance Observer Design

With the inverse and the other filters specified in Fig. 2, it remains to design $Q(z^{-1})$, which is the heart of the selective model inversion and disturbance observer. For narrow-band vibrations, there exist configurations that can achieve optimal disturbance rejection.

Recall (1). To regulate $y(k) = S(q^{-1})d(k)$ to zero, it suffices to design $Q(z^{-1})$ such that at the steady state

$$\left(1 - q^{-m}Q(q^{-1})\right)d(k) = 0. \tag{8}$$

We propose an IIR structure $Q(z^{-1}) = B_Q(z^{-1})/A_Q(z^{-1})$. For a vibration disturbance that is composed of $d(k) = \sum_{i=1}^{n} C_i \sin(\omega_i k + \psi_i)$ ($C_i \neq 0$, $\omega_i \neq 0$, $\psi_i \in \mathcal{R}$), it can be verified that, after two steps of transient, $\left(1 - 2\cos(\omega_i)q^{-1} + q^{-2}\right)C_i \sin(\omega_i k + \psi_i) = 0$. This is the concept of the intern model principle [5], [27]. Define

$$A(z^{-1}) \triangleq \prod_{i=1}^{n}(1 - 2\cos(\omega_i)z^{-1} + z^{-2}), \tag{9}$$

then

$$\begin{aligned} A(q^{-1})d(k) &= \sum_{i=1}^{n}\prod_{j=1}^{n}(1 - 2\cos\left(\omega_j\right)q^{-1} + q^{-2})C_i \sin(\omega_i k + \psi_i) \\ &= \sum_{i=1}^{n}\left(\prod_{j=1,\ j\neq i}^{n}(1 - 2\cos\left(\omega_j\right)q^{-1} + q^{-2})\right)\times \\ &\qquad (1 - 2\cos(\omega_i)q^{-1} + q^{-2})C_i \sin(\omega_i k + \psi_i) \end{aligned}$$

is zero after $2n$ steps of transient, and (8) is achieved if

$$1 - z^{-m}Q(z^{-1}) = K(z^{-1})\frac{A(z^{-1})}{A_Q(z^{-1})}. \tag{10}$$

To get a $1 - z^{-m}Q(z^{-1})$ with a magnitude response similar to that in Fig. 3, $A(z^{-1})/A_Q(z^{-1})$ should have a notch-filter structure. A natural choice is to damp the roots of $A(z^{-1})$ by a scalar $\alpha \in (0,1)$ and let

$$A_Q(z^{-1}) \triangleq \prod_{i=1}^{n}\left(1 - 2\alpha\cos(\omega_i)z^{-1} + \alpha^2 z^{-2}\right), \tag{11}$$

i.e., $A_Q(z^{-1}) = A(\alpha z^{-1})$. This makes $Q(z^{-1})$ stable, and will benefit the parameter adaptation algorithm later. To see the latter point, expanding the product in (9), we can get

$$A(z^{-1}) = 1 + a_1 z^{-1} + \cdots + a_n z^{-n} + \cdots + a_1 z^{-2n+1} + z^{-2n}, \tag{12}$$

where we have mapped the parameters $\{\omega_i\}_1^n$ in (9) to $\{a_i\}_1^n$, and the new coefficient vector $\{1, a_1, \ldots, a_n, \ldots, a_1, 1\}$ has a mirror symmetric form by construction. Replacing every z^{-1} with αz^{-1}, we obtain $A_Q(z^{-1}) = A(\alpha z^{-1})$, which is also linear in $\{a_i\}_1^n$. Only these n parameters need to be later identified. This is the minimum possible number for n unknown narrow-band signals.

The filter $K(z^{-1})$ is necessary to make the solution causal for a general m. Without $K(z^{-1})$, (10) indicates that $Q(z^{-1}) = z^m(A_Q(z^{-1}) - A(z^{-1}))/A_Q(z^{-1})$, where the non-realizable z^m is non-trivial to cancel. A design guide for $K(z^{-1})$ is that it should not introduce serious magnitude distortion to the achieved notch shape of $A(z^{-1})/A(\alpha z^{-1})$ in $1 - z^{-m}Q(z^{-1}) = K(z^{-1})A(z^{-1})/A(\alpha z^{-1})$. This way we can control the noise amplification in (8), especially when $d(k)$ contains other disturbances not modeled by (9). We discuss next choices of $K(z^{-1})$ for different values of m.

A. The case for $m = 0$

For the simplest case $m = 0$, a scalar value $K(z^{-1}) = k_0$ provides a realizable solution to (10). Recalling $Q(z^{-1}) = B_Q(z^{-1})/A_Q(z^{-1}) = B_Q(z^{-1})/A(\alpha z^{-1})$ and (12), we reduce (10) to $A(\alpha z^{-1}) - B_Q(z^{-1}) = k_0 A(z^{-1})$, which yields

$$\begin{aligned} B_Q(z^{-1}) = (1 - k_0) + (\alpha - k_0)a_1 z^{-1} + \cdots + (\alpha^n - k_0)a_n z^{-n} + \\ \cdots + (\alpha^{2n-1} - k_0)a_1 z^{-2n+1} + (\alpha^{2n} - k_0)z^{-2n}. \end{aligned} \tag{13}$$

It can be shown (see Appendix) that $k_0 = \alpha^n$ leads to the common factor $1-\alpha z^{-2}$ in $B_Q(z^{-1})$, which places two symmetric zeros to $Q(z^{-1})$ at $\pm\sqrt{\alpha}$. This provides balanced magnitude response for $Q(z^{-1})$ at low and high frequencies.

B. The case for $m = 1$

Applying analogous analysis as in Section IV-A, if $m = 1$, we reduce (10) to $A(\alpha z^{-1}) - z^{-1}B_Q(z^{-1}) = k_0 A(z^{-1})$, the solution of which is $B_Q(z^{-1}) = (1-k_0)z + (\alpha-k_0)a_1 + \cdots + (\alpha^n - k_0)a_n z^{-n+1} + \cdots + (\alpha^{2n-1} - k_0)a_1 z^{-2n+2} + (\alpha^{2n} - k_0)z^{-2n+1}$.

To let the term $(1-k_0)z$ vanish for realizability, we require $k_0 = 1$, which gives

$$B_Q(z^{-1}) = \sum_{i=1}^{2n} (\alpha^i - 1)a_i z^{-i+1};\ a_i = a_{2n-i},\ a_{2n} = 1. \tag{14}$$

As an example, when $n = 1$, (9), (12) and (14) yield $a_1 = -2\cos\omega_1$ and

$$Q(z^{-1}) = \frac{(1-\alpha)\left(2\cos\omega_1 - (1+\alpha)z^{-1}\right)}{1 - 2\alpha\cos\omega_1 z^{-1} + \alpha^2 z^{-2}}.$$

Evaluating the frequency response at ω_1 and using the identity $2\cos(\omega_1) = e^{j\omega_1} + e^{-j\omega_1}$, we can obtain that $Q(e^{-j\omega_1}) = e^{j\omega_1}$. Thus, $Q(z^{-1})$ provides exactly one-step advance to counteract the one-step delay in $1 - z^{-1}Q(z^{-1})$ at the center frequency ω_1, hence the zero magnitude response of $1 - z^{-1}Q(z^{-1})$ at ω_1.

C. The case for an arbitrary m

For $m > 1$, assigning $K(z^{-1}) = k_0$ no longer gives a realizable solution. Defining $K(z^{-1})$ as a general FIR filter can address the causality issue. This will give slightly less control over the shape of $K(z^{-1})A(z^{-1})/A(\alpha z^{-1})$, as $K(z^{-1})$ is now an FIR to be computed and its shape is non-trivial until we have solved (10). Another way that provides additional design freedom is to consider an IIR design:

$$K(z^{-1}) = \sum_{i=0}^{N} k_i \left[\frac{A(z^{-1})}{A(\alpha z^{-1})}\right]^i,\ k_i \in \mathcal{R}. \tag{15}$$

Namely, $K(z^{-1})$ is chosen as a combination of $N(\geq 0)$ filters that influence only the local loop shape (recall that $A(z^{-1})/A(\alpha z^{-1})$ is a notch filter). Take the example of $m = 2$. When $N = 1$,[1] (10) is

$$1 - z^{-2}Q(z^{-1}) = \left(k_0 + k_1\frac{A(z^{-1})}{A(\alpha z^{-1})}\right)\frac{A(z^{-1})}{A(\alpha z^{-1})},$$

which gives

$$Q(z^{-1}) = z^2\left(1 - k_0\frac{A(z^{-1})}{A(\alpha z^{-1})} - k_1\frac{A(z^{-1})^2}{A(\alpha z^{-1})^2}\right). \tag{16}$$

Partitioning, we obtain

$$Q(z^{-1}) \triangleq z^2\left(1 - \rho_1\frac{A(z^{-1})}{A(\alpha z^{-1})}\right)\left(1 - \rho_2\frac{A(z^{-1})}{A(\alpha z^{-1})}\right). \tag{17}$$

[1] If $N = 0$, the result is unrealizable since $K(z^{-1})$ is a scalar again.

The numerator of $Q(z^{-1})$ is given by $B_Q(z^{-1}) = z^2(A(\alpha z^{-1}) - \rho_1 A(z^{-1}))(A(\alpha z^{-1}) - \rho_2 A(z^{-1}))$. Recalling (12), we have $A(\alpha z^{-1}) - \rho_i A(z^{-1}) = (1-\rho_i) + (\alpha - \rho_i)a_1 z^{-1} + \cdots + (\alpha^{2n} - \rho_i)z^{-2n}$. To make the z^2 term vanish in $B_Q(z^{-1})$ for realizability of $Q(z^{-1})$, we must have $1 - \rho_i = 0$ for $i = 1, 2$, yielding $k_0 = 2$, $k_1 = -1$ in (16). With these solved ρ_i and k_i, after simplification, (17) and (15) become

$$Q(z^{-1}) = \left[\frac{\sum_{i=1}^{2n}(\alpha^i - 1)a_i z^{-i+1}}{A(\alpha z^{-1})}\right]^2;\ a_i = a_{2n-i},\ a_{2n} = 1 \tag{18}$$

$$K(z^{-1}) = 2 - \frac{A(z^{-1})}{A(\alpha z^{-1})}. \tag{19}$$

For a general integer m, when $N = m - 1$, applying analogous analysis, we get the following partitioned $Q(z^{-1})$ from (15) and (10):

$$Q(z^{-1}) = z^m \prod_{i=1}^{m}\left(1 - \rho_i\frac{A(z^{-1})}{A(\alpha z^{-1})}\right).$$

The solution pair is thus obtained when $\rho_i = 1\ \forall i$, and

$$Q(z^{-1}) = \left[\frac{\sum_{i=1}^{2n}(\alpha^i - 1)a_i z^{-i+1}}{A(\alpha z^{-1})}\right]^m \tag{20}$$

$$1 - z^{-m}Q(z^{-1}) = 1 - \left(1 - \frac{A(z^{-1})}{A(\alpha z^{-1})}\right)^m \tag{21}$$

$$= \frac{A(z^{-1})}{A(\alpha z^{-1})}\sum_{i=1}^{m}\binom{m}{i}\left[-\frac{A(z^{-1})}{A(\alpha z^{-1})}\right]^{i-1}. \tag{22}$$

Here a_i is as defined in (18); and from (21) to (22) we have used the identity $(1+x)^m = 1 + \binom{m}{1}x + \cdots + \binom{m}{m}x^m$, where $\binom{m}{i} = \frac{m!}{i!(m-i)!}$ is the binomial coefficient.

It can be observed that the general result obtained here is essentially a cascaded version of the developed $Q(z^{-1})$ in Section IV-B. For the sake of clarity, we denote now the Q filter for $m = 0$ and $m = 1$ respectively as $Q_0(z^{-1})$ and $Q_1(z^{-1})$. From the discussion at the end of Section IV-B, $Q_1(z^{-1})$ provides one-step phase advance at the disturbance frequencies $\{\omega_i\}_1^n$, to address the term z^{-1} in $1 - z^{-1}Q_1(z^{-1})$. For a general m, we see that the cascaded $Q(z^{-1}) = \left[Q_1(z^{-1})\right]^m$ in (20) works the same way since $1 - z^{-m}Q(z^{-1}) = 1 - (z^{-1}Q_1(z^{-1}))^m$, i.e., each $Q_1(z^{-1})$ block compensates one z^{-1} term, to achieve $1 - e^{-jm\omega}Q(e^{-j\omega}) = 0$ when $\omega \in \{\omega_i\}_1^n$. Recall from Fig. 3, that $Q(z^{-1})$ is a special type of bandpass filter. Cascading multiple $Q_1(z^{-1})$ together not only provides the compensation for z^{-m}, but also provides an enhanced bandpass frequency response, as $|Q(e^{-j\omega})|^m \leq |Q(e^{-j\omega})|$ if $m \geq 1$ and $|Q(e^{-j\omega})| < 1$ (when ω is outside of the passband). If needed, we can additionally cascade one or multiple blocks of $Q_0(z^{-1})$ to $Q(z^{-1})$, which will further reduce the magnitude of the filter outside the passband.

V. Parameter Adaptation

This section discusses the online adaptation of $Q(z^{-1})$ when the disturbance characteristics is not known. Recall

from Fig. 2, that the residual is

$$y(k) = G_{d2y}(q^{-1})d(k) = S(q^{-1})d(k) \approx \frac{1-q^{-m}Q(q^{-1})}{1+P(q^{-1})C(q^{-1})}d(k).$$

The beginning of Section II has discussed the obtaining of $\hat{d}(k) \approx d(k)$. Letting $w(k) \triangleq \hat{d}(k)/(1+P(q^{-1})C(q^{-1}))$ and recalling the solution of $1-q^{-m}Q(q^{-1})$ in (22), we get

$$y(k) \approx \left\{\sum_{i=1}^{m}\begin{pmatrix} m \\ i \end{pmatrix}\left[-\frac{A(q^{-1})}{A(\alpha q^{-1})}\right]^{i-1}\right\}\frac{A(q^{-1})}{A(\alpha q^{-1})}w(k)$$

The direct dynamics between $w(k)$ and $y(k)$ is nonlinear w.r.t. the unknown coefficients $\theta \triangleq [a_1, a_2, \ldots, a_n]^T$ in $Q(z^{-1})$. Noticing however the filter $\sum_{i=1}^{m}\begin{pmatrix} m \\ i \end{pmatrix}\left[-\frac{A(q^{-1})}{A(\alpha q^{-1})}\right]^{i-1}$ is a linear combination of (and actually also normalized) notch filters,[2] we can simply design to minimize

$$\tilde{y}(k) = A(q^{-1})/A(\alpha q^{-1})w(k). \tag{23}$$

Additional filtering can be applied on $w(k)$ to improve the signal-to-noise ratio. In the benchmark, the interested disturbance-rejection region is [50–95] Hz. A bandpass filter in Fig. 4 can be used on $w(k)$.

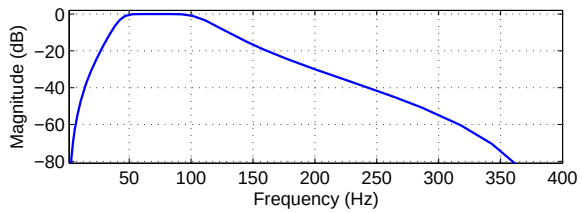

Figure 4: Example bandpass filter

The structure of (23) is special (and simplified) for adaptive control due to the close relationship between the numerator and the denominator. For such type of adaptation model, [2] has proposed a two-stage adaptation scheme that combines recursive least squares and output-error based parameter adaptation algorithms (PAA) for identification of θ. We list below only the central equations and then focus on applying the PAA for identifying different time-varying vibrations.

Step one: recursive least squares (RLS) aiming at minimizing $A(q^{-1})w(k)$, where $A(q^{-1})$ is given by (12):

$$\epsilon^o(k) = -\hat{A}(q^{-1})w(k) \tag{24}$$

$$= -\psi(k-1)^T\hat{\theta}(k-1) - (w(k)+w(k-2n)) \tag{25}$$

$$\hat{\theta}(k) = \hat{\theta}(k-1) + \frac{P(k-1)\psi(k-1)\epsilon^o(k)}{1+\psi(k-1)^T P(k-1)\psi(k-1)} \tag{26}$$

$$P(k) = \frac{1}{\lambda(k)}\left[P(k-1) - \frac{P(k-1)\psi(k-1)\psi^T(k-1)P(k-1)}{\lambda(k)+\psi^T(k-1)P(k-1)\psi(k-1)}\right]$$

Here the regressor vector $\psi(k-1) = [\psi_1(k-1), \ldots, \psi_n(k-1)]^T$ is computed from $\psi_i(k-1) = w(k-i) + w(k-2n+i)$; $i = 1, \ldots, n-1$, and $\psi_n(k-1) = w(k-n)$.

[2] In special case where $m = 1$, this summation term becomes identity.

Step two: parallel adaptation algorithm with a fixed compensator $C(z^{-1}) = 1 + c_1\alpha z^{-1} + \cdots + c_n\alpha^n z^{-n} + \cdots + c_1\alpha^{2n-1}z^{-2n+1} + \alpha^{2n}z^{-2n}$, aiming at minimizing $A(q^{-1})/A(\alpha q^{-1})w(k)$. With the newly introduced denominator part, the regressor vector is composed of $\phi_i(k-1) = w(k-i) + w(k-2n+i) - \alpha^i e(k-i) - \alpha^{2n-i}e(k-2n+i)$; $i = 1, \ldots, n-1$, and $\phi_n(k-1) = w(k-n) - \alpha^n e(k-n)$. We have

$$e(k) = \phi(k-1)^T\hat{\theta}(k) + w(k) + w(k-2n) - \alpha^{2n}e(k-2n)$$

$$\nu(k) = C(q^{-1})e(k) = e(k) + \alpha^{2n}e(k-2n) + \varphi(k-1)^T\theta_c \tag{27}$$

$$e^o(k) = \phi(k-1)^T\hat{\theta}(k-1) + w(k) + w(k-2n) - \alpha^{2n}e(k-2n)$$

$$\nu^o(k) = e^o(k) + \alpha^{2n}e(k-2n) + \varphi(k-1)^T\theta_c \tag{28}$$

where $e(k)$ and $\nu(k)$ are respectively the *a posteriori* estimation and adaptation errors; $e^o(k)$ and $\nu^o(k)$ are respectively the *a priori* estimation and adaptation errors; and $\theta_c \triangleq [c_1, c_2, \ldots, c_n]$ is the coefficient vector of $C(z^{-1})$. $\varphi(k-1) = [\varphi_1(k-1), \varphi_2(k-1), \ldots, \varphi_n(k-1)]^T$ in (27) and (28) are computed from: $\varphi_i(k-1) = \alpha^i e(k-i) + \alpha^{2n-i}e(k-2n+i)$; $i = 1, \ldots, n-1$, $\varphi_n(k-1) = \alpha^n e(k-n)$. The final parameter adaptation equations are

$$\hat{\theta}(k) = \hat{\theta}(k-1) + \frac{P(k-1)\left(-\phi(k-1)\right)\nu^o(k)}{1+\phi(k-1)^T P(k-1)\phi(k-1)} \tag{29}$$

$$P(k) = \frac{1}{\lambda(k)}\left[P(k-1) - \frac{P(k-1)\phi(k-1)\phi^T(k-1)P(k-1)}{\lambda(k)+\phi^T(k-1)P(k-1)\phi(k-1)}\right]$$

The RLS algorithm is globally convergent if the adaptation input contains pure narrow-band vibrations, but yields biased estimate if there are colored input noises. The parallel algorithm in Step two provides accurate local convergence but needs proper parameter initialization. Steps one and two are therefore connected by using the final estimated parameter $\hat{\theta}^o$ at Step one to initialize θ_c and $\hat{\theta}$ in Step two. The switching between the two steps can be made automatic [2] (after some tuning) or simply by a fixed time window to run Step one.

To have good convergence under noisy environments, let α in Step two initialize from a relatively small value (e.g. 0.8) and converge gradually to a value that is close to 1 (e.g. 0.99). The estimated $\hat{\theta}(k)$ is then used to construct the Q filter designed in the previous section (the coefficient α in the Q filter for implementation does not need to be the same as that used in parameter adaptation).

The forgetting factor $\lambda(k)$ determines how much information is used for adaptation. In this article we suggest the following tuning rules:

(i) rapid initial convergence: initialize the forgetting factor to be exponentially increasing from λ_0 to 1 in the first several samples, where λ_0 can be taken to be between $[0.92, 1)$

(ii) adjustment for sudden parameter change: when the prediction error encounters a sudden increase, indicating a change of system parameters, switch from Step two to Step one, reduce $\lambda(k)$ to a small value $\underline{\lambda}$ (e.g. 0.92

in the benchmark), and then increase it back to its steady-state value $\overline{\lambda}$ (usually close to 1), using the formula $\lambda(k) = \overline{\lambda} - \lambda_{\text{rate}}(\overline{\lambda} - \lambda(k-1))$, with λ_{rate} [preferably in the range $(0.9, 0.995)$] defining the speed of convergence.

(iii) adjustment for continuously changing parameters: when the parameters are changing, keep $\lambda(k)$ strictly smaller than one, using e.g., a constant $\lambda(k)(<1)$.

VI. Implementation

In this section we provide some details about implementing the algorithm:

Obtaining the frequencies from the identified parameters: from (9) and (12), the vibration frequencies and the identified parameters are mapped by $\prod_{i=1}^{n}\left(1-2\cos(\omega_i)z^{-1}+z^{-2}\right) = 1 + a_1 z^{-1} + \cdots + a_n z^{-n} + \cdots + a_1 z^{-2n+1} + z^{-2n}$. For the simplest case where $n = 1$, we have $a_1 = -2\cos\omega_1$, from which we can compute the vibration frequency $\omega_1 = 2\pi\Omega_1 T_s$, where the unit of Ω_1 is Hz. The parameter a_1 is online updated and Ω_1 can be computed offline for algorithm tuning. For $n > 1$, as $\left(1-2\cos(\omega_i)z^{-1}+z^{-2}\right) = \left(1-e^{j\omega_i}z^{-1}\right)\left(1-e^{-j\omega_i}z^{-1}\right)$, ω_i can be computed offline via calculating the angle of the complex roots of $1+a_1 z^{-1}+\cdots+a_n z^{-n}+\cdots+a_1 z^{-2n+1}+z^{-2n} = 0$.

Algorithm tuning: besides the above structural mapping between the identified parameters and the vibration frequency, another property is also useful for algorithm tuning: the width of the attenuation bandwidth in Fig. 3 is determined by the parameter α in (11). When α is smaller but very close to one, the magnitude of $Q(z^{-1})$ is very small except at the vibration frequencies. The closed-loop robust stability will then be easy to satisfy from Theorem 1. This will however require very accurate information of the disturbance frequency. Designers can gradually reduce α to reach the desired attenuation bandwidth. Keep in mind, however, that the Q filter should satisfy the gain constraint (4) for stability.

Baseline controller: the active suspension system is open-loop stable. Since the benchmark is on narrowband vibration rejection rather than motion control, we used a baseline controller (provided by the benchmark[3]) that has very small gains to achieve closed-loop robust stability. For general motion control problems, the baseline controller should also be carefully chosen to provide the standard loop-shaping performance (see, e.g., [2]).

VII. Simulation and Experimental Results

We apply in this section the proposed scheme to the benchmark on active suspension. In this system, the plant delay $m = 2$ in the modeling of $P(z^{-1})\big|_{z=e^{j\omega}} \approx z^{-m}P_m(z^{-1})\big|_{z=e^{j\omega}}$. Hence two $Q_1(z^{-1})$ blocks are needed in (20). Vibrations occur in the middle frequency region between 50 Hz and 95 Hz. There are also other noises at low and high frequencies. To enhance the bandpass property of $Q(z^{-1})$, we added one additional $Q_0(z^{-1})$ block designed in Section IV-A, and prefiltered the input to the PAA by a bandpass filter as shown in Fig. 4 to remove the bias and other high-frequency noises in the estimated disturbance. Three levels of evaluations are conducted. Within each level, three types of disturbances are considered: the first with constant unknown frequencies injected at a certain time (denoted as simple step test), the second with sudden frequency changes at specific time instances, and the third with chirp-changing frequencies. The graphical and numerical data are compared to other participants of the benchmark.

[3]See http://www.gipsa-lab.grenoble-inp.fr/~ioandore.landau/benchmark_adaptive_regulation/index.html

A. Level 1: rejection of single-frequency vibrations

Fig. 5 shows the time trace of the residual errors (experimental result) for a time-varying vibration with the following characteristics: the disturbance frequency changes in the pattern of null→ 75Hz→ 85Hz→ 75Hz→ 65Hz→ 75Hz→ null, occurring respectively at 5 sec, 8 sec, 11 sec, 14 sec, 17 sec, and finally 32 sec, when the disturbance is turned off. In the presence of various frequency jumps, the algorithm is seen to provide rapid and strong vibration compensation. Comparing the data at 2 sec and 7 sec, we see that the steady-state residual errors with the compensation scheme (data at 7 sec) has been reduced to be at the same magnitude as the baseline case (at 2 sec) where no disturbance is present. Summarized in Table I are the simulation and experimental results of a full set of evaluations covering different frequency values. The performance is evaluated by two quantitative values: the 2-norm values of the transient errors at the initial 3 seconds after disturbance injection (denoted as $\|e\|_2^2$ Ⓣ), and the maximum values of the residual error. It can be seen the performances at different frequencies are all similar to that in Fig. 5.

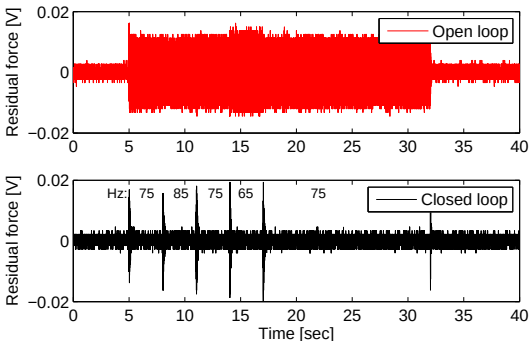

Figure 5: **Experimental** results of rejecting a narrowband disturbance with step frequency changes.

At a particular frequency, Fig. 6 presents the steady-state error spectra when the system is subjected to a 75-Hz disturbance. With the compensation scheme, the spectral peak at 75 Hz has been reduced from around −42 dB to −91 dB, indicating a disturbance attenuation of about 49 dB (the benchmark specification is 40 dB). These results are directly reflected in Fig. 7, which presents the magnitude responses of the sensitivity functions

Table I: Results of rejecting vibrations with step changes in frequencies (level 1)

		freq. (Hz)	$\|e\|_2^2$ Ⓣ ($\times 10^{-3}$V^2)	max$\|e\|$ ($\times 10^{-3}$V)
Simulation	Seq. 1	60→70	20.78	22.10
		70→60	11.21	19.80
		60→50	15.51	19.40
		50→60	10.39	20.98
	Seq. 2	75→85	19.29	22.43
		85→75	10.12	17.37
		75→65	10.66	18.96
		65→75	9.09	19.17
	Seq. 3	85→95	17.09	23.93
		95→85	12.13	23.02
		85→75	10.15	18.96
		75→85	8.64	16.93
Experiment	Seq. 1	60→70	19.50	23.95
		70→60	13.51	20.27
		60→50	28.47	23.85
		50→60	15.62	22.62
	Seq. 2	75→85	16.64	20.16
		85→75	9.93	16.61
		75→65	11.31	20.28
		65→75	10.11	18.93
	Seq. 3	85→95	135.00	25.18
		95→85	16.07	19.06
		85→75	10.33	18.94
		75→85	8.56	15.26

(note the sharp notch at 75 Hz and small amplifications at other regions). During actual experiments there are random noises that are time-dependent. Hence comparing to Fig. 6a, the open- and closed-loop spectra, at frequencies other than the spectral peaks, look slightly more different in Fig. 6b.

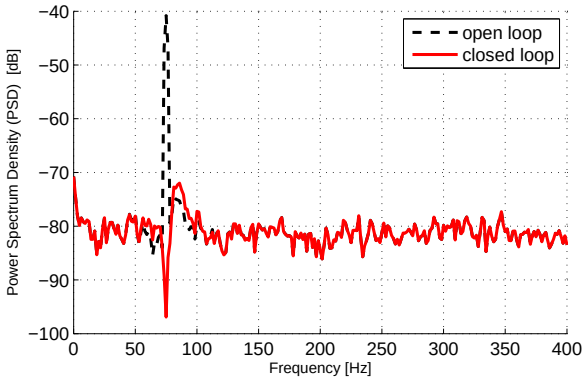

(a) Simulation

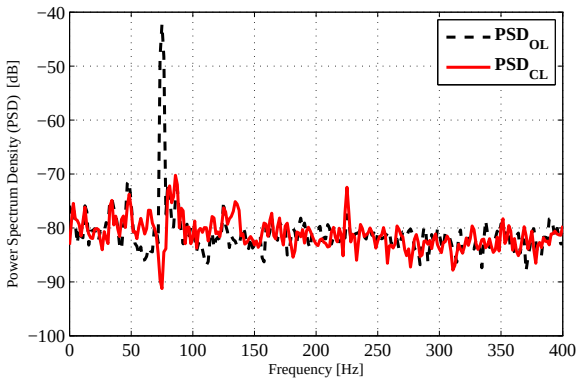

(b) Experiment

Figure 6: Error spectra of rejecting a 75 Hz vibration

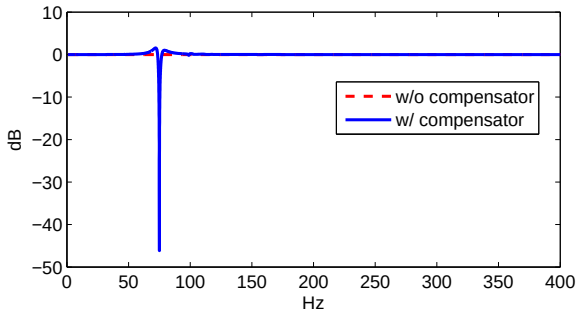

Figure 7: Magnitude response of the sensitivity functions with (w/) and without (w/o) the proposed compensator

The algorithm is additionally tested at frequencies uniformly sampled between 50 Hz and 95 Hz. Table II summarizes, from the second to the last columns, the overall 2-norm reduction of the errors (global attenuation **GA**), the disturbance attenuation (**DA**) at the vibration frequencies, the maximum spectral amplification, the 3-sec transient value of $\|e\|_2^2$ Ⓣ, the residual value of $\|e\|_2^2$ at the final 3 seconds (denoted as $\|e\|_2^2$ Ⓡ), the maximum of $|e|$, and lastly a scalar called transient ratio (**T ratio**). T ratio is the ratio between $\|e\|_2^2$ at two time windows: the first from 7 sec to 10 sec (disturbance was injected at 5 sec); the other at the final 3 seconds. It is a measure of whether the residual errors have converged to the steady-state values after two seconds (required specification from benchmark) of running the adaptive algorithm. If T ratio is less than 1.21, it is regarded that the algorithm has fully converged (100% satisfaction in the benchmark). The numbers indicate that, similar to the case in Fig. 6, in all tests, the narrow-band disturbance has been greatly attenuated within a short period of time. As the system has two pairs of strong resonant and anti-resonant modes neat 50 Hz and 100 Hz (recall Fig. 1), we intentionally reduced the depth of attenuation at frequencies below 52 Hz and above 92 Hz in the experiments. This is done by selecting α to be closer to 1, and hence a sharper notch shape in Fig. 3. The simulation results do not have this modification and reflect the best possible performance.

Fig. 8 shows a summary, in the same scale, of the level-1 time-domain results under different specifications. The first subplot is the time-domain result corresponding to the spectra in Fig. 6; and the second subplot is another example with step frequency changes in the disturbance. The third one is for the case when the disturbance is a chirp signal whose frequency sweeps between 50 Hz and 95 Hz in the time windows {[10–15], [20–25]} sec. Under such time-varying vibrations, we see that the proposed algorithm maintains its effectiveness of compensating the disturbance. For this time-varying vibration, we used an aggressive forgetting factor to track the changing frequency, to achieve a compensation result that is as good as those in the first two subplots. Yet the parameter was updated a bit too fast when the vibration stopped changing its frequency from 15 sec to 20 sec (recall that

Table II: Results of rejecting vibrations with unknown constant frequencies (level 1 simple step test)

	freq. (Hz)	GA (dB)	DA (dB)	max. amp. (dB)	max. amp. @(Hz)	$\|e\|_2^2$ ① ($\times 10^{-3}$V^2)	$\|e\|_2^2$ ® ($\times 10^{-3}$V^2)	max$\|e\|$ ($\times 10^{-3}$V)	T ratio
Simulation	50	34.55	51.18	3.10	60.94	10.09	3.62	18.29	1.0571
	55	34.40	56.55	4.04	46.88	8.66	3.73	20.68	1.0574
	60	34.40	52.22	3.33	50.00	8.17	3.71	20.53	1.0684
	65	34.43	50.93	3.08	54.69	8.01	3.71	19.78	1.0575
	70	34.44	55.44	2.79	81.25	8.03	3.83	20.00	1.0515
	75	34.77	54.76	2.96	67.19	8.46	3.73	19.27	1.0511
	80	34.99	46.99	3.74	100.00	8.89	3.67	21.64	1.0605
	85	34.62	45.87	4.88	100.00	9.72	3.64	23.80	1.0588
	90	32.53	45.83	4.25	101.56	10.78	3.81	27.15	1.0444
	95	25.39	48.33	4.72	103.13	13.97	3.82	29.54	1.0753
Experiment	50	35.80	46.61	7.58	62.50	14.79	6.20	29.21	0.9999
	55	35.43	51.38	10.91	128.10	11.63	4.67	19.00	0.9106
	60	35.51	52.10	8.89	128.10	11.26	4.02	19.00	1.0987
	65	33.54	53.89	7.52	75.00	10.56	4.17	17.81	0.9784
	70	31.42	48.37	8.02	117.20	10.33	4.45	19.03	1.0186
	75	31.05	49.01	7.85	135.90	10.18	4.11	17.81	1.0119
	80	31.44	49.04	9.29	289.10	10.71	3.79	20.28	0.9905
	85	30.23	45.70	6.63	126.60	11.19	4.04	19.08	0.9993
	90	29.40	42.62	8.20	129.70	12.33	3.89	21.49	0.9933
	95	26.42	31.58	6.64	0.10	18.04	4.33	26.30	1.0434

95 Hz is close to the sharp resonant mode). In level two and level three, the adaptation speed was reduced to give a smoother overall transient. Table III summarizes, for all three levels of evaluations, the maximum of the absolute error and the mean square error value $E(e^2)$ for rejecting the chirp disturbances. These numbers are all within the benchmark specifications.

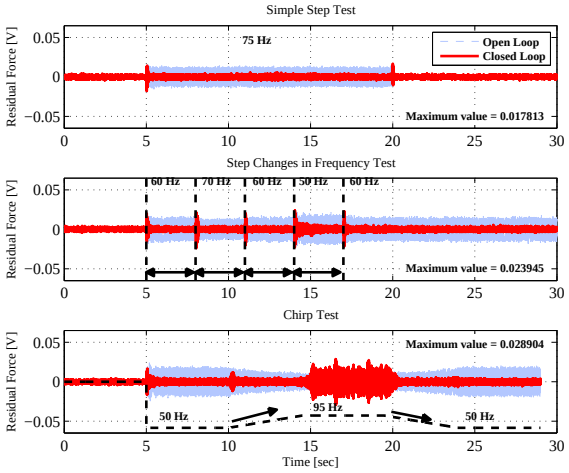

Figure 8: Time-domain level-1 **experimental** results

Table III: Simulation (Sim.) and experimental (Exp.) results of rejecting chirp disturbances

		max$\|e\|$ ($\times 10^{-3}$V)		$E(e^2)$ ($\times 10^{-6}$V^2)	
	Freq.	↗	↘	↗	↘
Sim.	Level 1	8.8	5.3	3.83	2.91
	Level 2	34.4	96.5	87.5	407
	Level 3	38.0	38.5	197	193
Exp.	Level 1	20.3	11.7	4.37	11.5
	Level 2	31.5	33.9	79.8	61.5
	Level 3	33.6	41.2	102	111

B. Level-2: rejection of two narrow-band vibrations

In level 2 the complexity of the test was doubled. Figs. 9 and 10 show, respectively, the frequency- and time-domain experimental results in one test. The algorithm is seen to have maintained its effectiveness and performance in rejecting the vibrations. Fig. 9 corresponds to the spectral comparison for the first subplot in Fig. 10. The disturbances at 60 and 80 Hz are attenuated, respectively, by 41.91 dB and 39.05 dB, without introducing large amplified errors at other frequencies. Indeed, the proposed algorithm has the property of maintaining very small amplification of other disturbances, due to the frequency-domain design criterion in Fig. 3. The full simulation and experimental results at different frequencies are summarized in Tables IV and V. Similar to level-1 results, the performance is uniform in different tests.

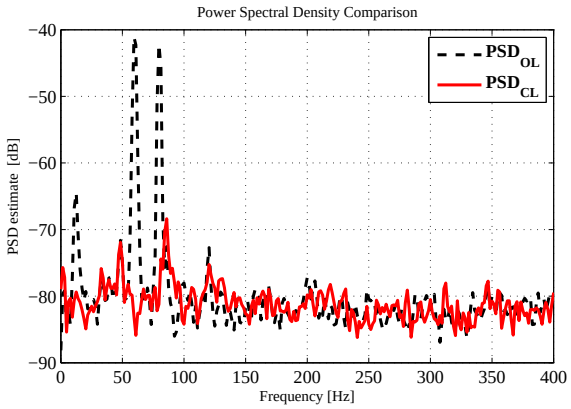

Figure 9: Frequency-domain level-2 **experimental** results

C. Level 3: rejection of three narrow-band vibrations

In this section the disturbance is extended to contain three narrow-band vibrations. Not only the complexity of the problem has been much increased, but also the adaptation environment is much more challenging. It

Table IV: Results of rejecting vibrations with unknown constant frequencies (level 2 simple step test)

	freq. (Hz)	GA (dB)	DA (dB)-(dB)	max. amp. (dB)	@(Hz)	$\|\|e\|\|_2^2$ ① ($\times 10^{-3}$V^2)	$\|\|e\|\|_2^2$ ® ($\times 10^{-3}$V^2)	max$\|e\|$ ($\times 10^{-3}$V)	T ratio
Simulation	50,70	39.87	(43.87)(49.81)	5.17	46.88	42.20	3.91	32.82	1.0542
	55,75	40.00	(51.22)(50.18)	3.83	100.00	29.20	3.93	30.31	1.0427
	60,80	40.35	(47.51)(42.28)	5.49	100.00	29.60	3.72	33.94	1.0533
	65,85	40.38	(46.66)(42.15)	6.69	100.00	25.10	3.71	36.33	1.0368
	70,90	39.66	(50.24)(41.23)	6.06	101.56	36.70	3.74	44.61	1.0437
	75,95	37.33	(49.84)(43.08)	4.87	109.38	40.10	3.73	44.40	1.0525
Experiment	50,70	37.56	(42.95)(45.04)	10.77	76.56	83.61	7.28	40.17	0.9276
	55,75	38.56	(47.11)(44.71)	7.98	115.63	52.38	5.15	31.69	0.9828
	60,80	39.83	(41.91)(39.05)	8.10	92.19	43.05	3.94	29.29	1.1452
	65,85	35.31	(50.39)(38.52)	11.27	104.69	42.63	5.74	31.76	1.0021
	70,90	37.05	(44.28)(37.33)	7.47	98.44	38.89	4.12	37.90	0.9652
	75,95	35.31	(46.31)(33.15)	9.04	71.88	42.24	4.55	39.16	1.1808

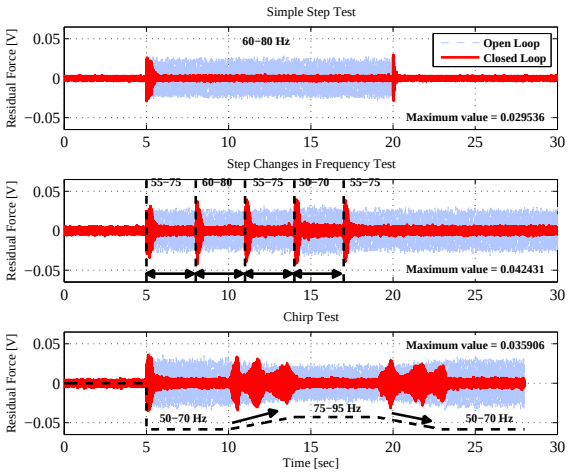

Figure 10: Time-domain level-2 **experimental** results

Table V: Results of rejecting vibrations with step changes in frequencies (level 2)

		freq. (Hz)	$\|\|e\|\|_2^2$ ① ($\times 10^{-3}$V^2)	max$\|e\|$ ($\times 10^{-3}$V)
Simulation	Seq. 1	[55,75]→[60,80]	52.60	34.30
		[60,80]→[55,75]	55.40	34.50
		[55,75]→[50,70]	70.40	36.70
		[50,70]→[55,75]	60.50	40.00
	Seq. 2	[70,90]→[75,95]	62.50	29.00
		[75,95]→[70,90]	53.60	36.40
		[70,90]→[65,85]	55.10	33.90
		[65,85]→[70,90]	45.60	31.80
Experiment	Seq. 1	[55,75]→[60,80]	64.54	42.43
		[60,80]→[55,75]	72.71	39.68
		[55,75]→[50,70]	102.45	41.21
		[50,70]→[55,75]	70.79	38.76
	Seq. 2	[70,90]→[75,95]	83.67	37.18
		[75,95]→[70,90]	56.23	40.02
		[70,90]→[65,85]	66.46	34.73
		[65,85]→[70,90]	85.89	38.80

appears the strong vibrations have excited other system modes at the beginning of all experiments (see the small side peaks in Fig. 11). Fig. 11 presents the error spectra in the scheme where the disturbance frequencies are unknown but constant. Similar to the case in previous sections, the narrow-band disturbances have been greatly attenuated. Some of the small side peaks, although not expected at the design stage, are actually attenuated in the experiments (similar result also appears in Fig. 9), and the proposed algorithm correctly found the largest peaks. Fig. 12 provides an example of the time-domain results at each disturbance characteristics. The corresponding identified frequencies for the second subplot are shown in Fig. 13 (computed offline from the method in Section VI). With the correctly identified frequencies, the algorithm rapidly reduces the residual errors to the same magnitude as the case where no vibrations are present.

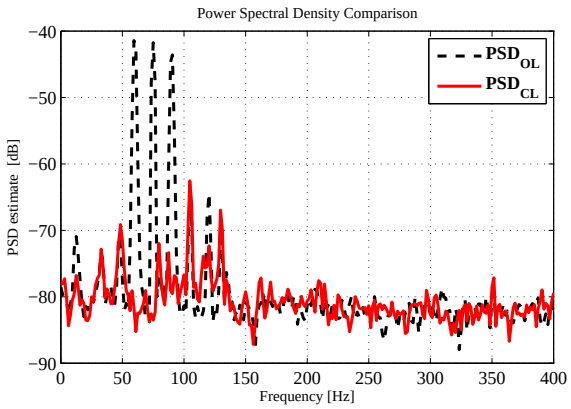

Figure 11: Error spectra in the rejection of three narrow-band vibrations (**experimental** result)

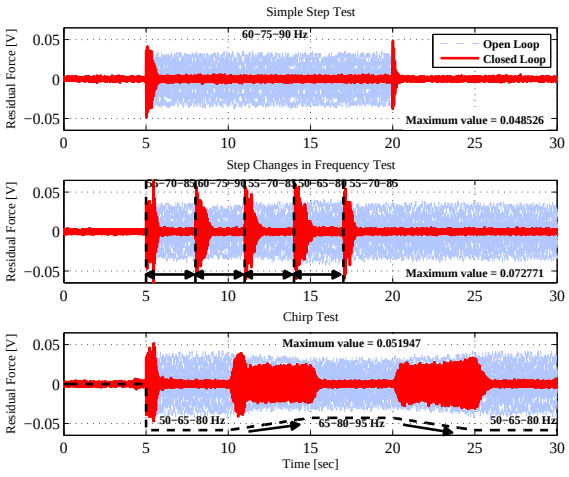

Figure 12: Time-domain level-3 **experimental** results

Table VI: Results of rejecting vibrations with unknown constant frequencies (level 3 simple step test)

	freq. (Hz)	GA (dB)	DA (dB)-(dB)-(dB)	max. amp. (dB)	max. amp. @(Hz)	$\|e\|_2^2$ ① ($\times 10^{-3}$)	$\|e\|_2^2$ ® ($\times 10^{-3}$)	max$\|e\|$ ($\times 10^{-3}$)	T ratio
Sim.	50,65,80	43.91	(42.63)(39.54)(40.76)	6.57	101.56	108.90	3.70	44.70	1.0835
	55,70,85	43.93	(47.93)(44.80)(40.36)	4.91	101.56	95.70	3.70	49.60	1.0518
	60,75,90	43.48	(45.57)(47.12)(40.29)	4.88	110.94	75.90	3.70	52.80	1.0488
	65,80,95	42.00	(44.58)(39.94)(41.39)	5.11	110.94	56.70	3.70	59.10	1.0422
Exp.	50,65,80	41.97	(38.48)(45.66)(42.86)	7.54	93.75	182.13	5.73	47.10	0.9911
	55,70,85	39.59	(44.79)(44.41)(37.54)	9.46	46.88	127.86	6.08	51.98	0.9675
	60,75,90	38.31	(42.65)(41.75)(35.95)	8.27	115.63	94.49	6.17	48.53	1.1593
	65,80,95	39.01	(43.70)(37.90)(33.14)	8.26	54.69	98.87	5.01	54.64	1.0608

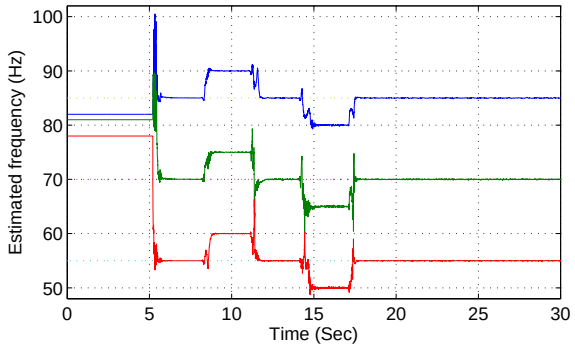

Figure 13: Identified frequencies for the middle plot of Fig. 12 (vibrations injected at the fifth second)

The full summary of simulation and experimental results at different frequencies are shown in Tables VI and VII. In all cases, the achieved performance are at the same level as those demonstrated in Figs. 11 to 13.

Table VII: Results of rejecting vibrations with step changes in frequencies (level 3)

		freq. (Hz)	$\|e\|_2^2$ ① ($\times 10^{-3}$V^2)	max$\|e\|$ ($\times 10^{-3}$V)
Simulation	Seq. 1	[55,70,85]→[60,75,90]	72.60	48.90
		[60,75,90]→[50,70,85]	80.11	54.11
		[55,70,85]→[50,65,80]	109.84	52.47
		[50,65,80]→[55,70,85]	76.17	49.10
	Seq. 2	[60,75,90]→[65,80,95]	60.81	44.51
		[65,80,95]→[60,75,90]	79.87	49.57
		[60,75,90]→[55,70,95]	93.96	56.69
		[55,70,85]→[60,75,90]	99.21	52.26
Experiment	Seq. 1	[55,70,85]→[60,75,90]	149.24	56.84
		[60,75,90]→[50,70,85]	162.04	59.58
		[55,70,85]→[50,65,80]	242.40	59.58
		[50,65,80]→[55,70,85]	127.32	59.58
	Seq. 2	[60,75,90]→[65,80,95]	162.60	51.94
		[65,80,95]→[60,75,90]	120.96	52.22
		[60,75,90]→[55,70,95]	158.29	59.58
		[55,70,85]→[60,75,90]	133.57	59.30

The benchmark has set up several evaluation quantities about overall performance, robustness, and complexity. The proposed algorithm achieved 100% in the benchmark specification index for transient performance; 100%, 100%, and 99.78% respectively in steady-state simulation performance; and ranked one, three, and two, respectively in experimental results. The recorded task execution time is also moderate among the benchmark participants. Detailed summaries and discussions are provided in the benchmark synthesis paper [23].

D. Remark about the simulation and experimental results

From the tables, the proposed algorithm is seen to be effective under all tests. The experimental results match well with the simulations, and we can obtain quite good guidance from the offline simulation. Due to the presence of system uncertainties and unmodeled noises, some experiments are slightly more difficult to perform, especially when the disturbance frequencies are close to the resonances at around 50 Hz and 100 Hz in Fig. 1. Actually, as the actual resonances have slightly different frequencies than those in simulation, the initial run of the experiments at 50 Hz and 95 Hz failed in the parameter adaptation. To cope with the problem, we first used a weak baseline controller such that the gain between the disturbance and the control input is very low at high frequencies and around the system modes (see Fig. 14). Additionally, two modifications can be made on the Q-filter design. The first is to make the Q filter have sharper passbands in Fig. 3. The second is to put a scalar gain that is smaller than one ahead of $Q(z^{-1})$. The effect of both modifications is to make $Q(z^{-1})$ pass less noises in the band-pass process. Accompanied by this increased robustness, is the requirement of more accurate parameter convergence in the first modification, or the loss of perfect disturbance property in the second relaxation. From an engineering point of view, perfect disturbance rejection may however not always be necessary. For example, an attenuation of around 35 dB can already make the error spectra relatively flat in Fig. 6.

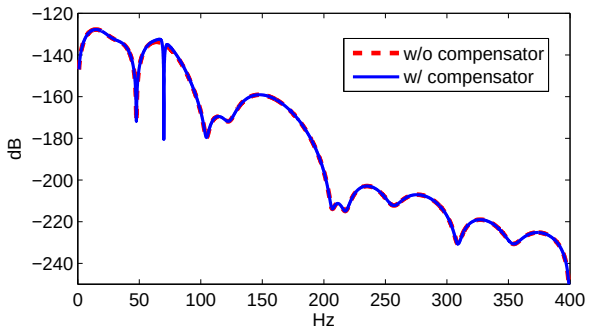

Figure 14: Magnitude response of the closed-loop transfer function from the disturbance to the control input

VIII. Conclusions

In this paper, an adaptive selective model inversion (SMI) scheme has been introduced for multiple narrow-band disturbance rejection. This special Youla parameterization is constructed by a H_∞-based inverse design and internal-model-principle based IIR filters. Under comprehensive tests, the proposed algorithm significantly attenuated the disturbance. In particular, the properties of minimum adaptation parameters, small error amplification, and intuitive tuning rules are useful for related control problems.

IX. Acknowledgment

We would like to thank Abraham Castellanos Silva for his help on the experiments. We would also like to thank Professor Landau for organizing the benchmark.

References

[1] I.-D. Landau, M. Alma, J.-J. Martinez, and G. Buche, "Adaptive suppression of multiple time-varying unknown vibrations using an inertial actuator," *IEEE Transactions on Control Systems Technology*, vol. 19, no. 6, pp. 1327–1338, 2011.

[2] X. Chen and M. Tomizuka, "A minimum parameter adaptive approach for rejecting multiple narrow-band disturbances with application to hard disk drives," *IEEE Transactions on Control Systems Technology*, vol. 20, pp. 408 – 415, March 2012.

[3] C. Kinney, R. de Callafon, E. Dunens, R. Bargerhuff, and C. Bash, "Optimal periodic disturbance reduction for active noise cancelation," *Journal of Sound and Vibration*, vol. 305, no. 1-2, pp. 22–33, Aug. 2007.

[4] L. Guo and Y. Chen, "Disk flutter and its impact on hdd servo performance," in *Proc. 2000 Asia-Pacific Magnetic Recording Conf.*, 2000, pp. TA2/1–TA2/2.

[5] B. Francis and W. Wonham, "The internal model principle of control theory," *Automatica*, vol. 12, no. 5, pp. 457–465, 1976.

[6] Q. Zhang and L. Brown, "Noise analysis of an algorithm for uncertain frequency identification," *IEEE Transactions on Automatic Control*, vol. 51, no. 1, pp. 103–110, 2006.

[7] W. Kim, H. Kim, C. Chung, and M. Tomizuka, "Adaptive output regulation for the rejection of a periodic disturbance with an unknown frequency," *IEEE Transactions on Control Systems Technology*, vol. 19, no. 5, pp. 1296–1304, 2011.

[8] F. Ben-Amara, P. T. Kabamba, and a. G. Ulsoy, "Adaptive sinusoidal disturbance rejection in linear discrete-time systems–part I: Theory," *ASME Journal of Dynamics Systems, Measurement, and Control*, vol. 121, no. 4, pp. 648–654, 1999.

[9] Y. Kim, C. Kang, and M. Tomizuka, "Adaptive and optimal rejection of non-repeatable disturbance in hard disk drives," in *Proc. 2005 IEEE/ASME International Conf. on Advanced Intelligent Mechatronics*, vol. 1, 2005, pp. 1–6.

[10] Q. Jia and Z. Wang, "A new adaptive method for identification of multiple unknown disturbance frequencies in hdds," *IEEE Transactions on Magnetics*, vol. 44, no. 11 Part 2, pp. 3746–3749, 2008.

[11] X. Chen and M. Tomizuka, "An indirect adaptive approach to reject multiple narrow-band disturbances in hard disk drives," in *Proc. 2010 IFAC Symposium on Mechatronic Systems, Sept. 13-15, 2010 Cambridge, Massachusetts, USA*, 2010, pp. 44–49.

[12] R. Roy and T. Kailath, "Esprit-estimation of signal parameters via rotational invariance techniques," *IEEE Transactions on Acoustics, Speech, and Signal Processing*, vol. 37, no. 7, pp. 984 –995, Jul. 1989.

[13] R. Schmidt, "Multiple emitter location and signal parameter estimation," *IEEE Transactions on Antennas and Propagation*, vol. 34, no. 3, pp. 276 – 280, Mar. 1986.

[14] A. Nehorai, "A minimal parameter adaptive notch filter with constrained poles and zeros," *IEEE Transactions on Acoustics, Speech, and Signal Processing*, vol. 33, no. 4, pp. 983–996, Aug. 1985.

[15] G. Obregon-Pulido, B. Castillo-Toledo, and A. Loukianov, "A globally convergent estimator for n-frequencies," *IEEE Transactions on Automatic Control*, vol. 47, no. 5, pp. 857 –863, May. 2002.

[16] L. Hsu, R. Ortega, and G. Damm, "A globally convergent frequency estimator," *IEEE Transactions on Automatic Control*, vol. 44, no. 4, pp. 698 –713, Apr. 1999.

[17] M. Mojiri and A. Bakhshai, "An adaptive notch filter for frequency estimation of a periodic signal," *IEEE Transactions on Automatic Control*, vol. 49, no. 2, pp. 314 – 318, Feb. 2004.

[18] B. Wu and M. Bodson, "A magnitude/phase-locked loop approach to parameter estimation of periodic signals," *IEEE Transactions on Automatic Control*, vol. 48, no. 4, pp. 612 – 618, Apr. 2003.

[19] R. Marino and P. Tomei, "Global estimation of n unknown frequencies," *IEEE Transactions on Automatic Control*, vol. 47, no. 8, pp. 1324 – 1328, Aug. 2002.

[20] R. Marino, G. L. Santosuosso, and P. Tomei, "Robust adaptive compensation of biased sinusoidal disturbances with unknown frequency," *Automatica*, vol. 39, no. 10, pp. 1755 – 1761, 2003.

[21] L. Ljung, *System Identification: Theory for the User*, 2nd ed. Prentice Hall PTR, 1999.

[22] X. Chen and M. Tomizuka, "Selective model inversion and adaptive disturbance observer for rejection of time-varying vibrations on an active suspension," in *2013 European Control Conf., July 17-19 (to appear)*.

[23] I.-D. Landau, A. C. Silva, T.-B. Airimitoaie, G. Buche, and M. Noe, "Benchmark on adaptive regulation – rejection of unknown/time-varying multiple narrow band disturbances," in *European Journal of Control, 2013 (to appear)*.

[24] S. Skogestad and I. Postlethwaite, *Multivariable Feedback Control: Analysis and Design*, 2nd ed. Wiley Chichester, UK, 2005.

[25] D. Youla, J. J. Bongiorno, and H. Jabr, "Modern wiener–hopf design of optimal controllers part i: The single-input-output case," *IEEE Transactions on Automatic Control*, vol. 21, no. 1, pp. 3–13, 1976.

[26] P. Overschee and B. Moor, *Subspace Identification for Linear Systems: Theory-Implementation-Applications*. Kluwer Academic Publishers, 1996.

[27] E. Davison, "The robust control of a servomechanism problem for linear time-invariant multivariable systems," *IEEE Transactions on Automatic Control*, vol. 21, no. 1, pp. 25–34, 1976.

Appendix

The Q-filter numerator in (13) can be partitioned into

$$B_Q\left(z^{-1}\right) = b_n z^{-n} + \sum_{i=0}^{n-1}\left(b_i z^{-i} + b_{2n-i} z^{-2n+i}\right), \qquad (30)$$

where $b_i = (\alpha^i - k)a_i$, $a_0 = 1$, and $a_i = a_{2n-i}$. Letting $k = \alpha^n$ gives $b_n = 0$ and

$$\begin{aligned} & b_i z^{-i} + b_{2n-i} z^{-2n+i} \\ =& \alpha^n a_i z^{-i}\left[\left(\alpha^{i-n} - 1\right) + \left(\alpha^{-i+n} - 1\right) z^{-2n+2i}\right] \end{aligned} \qquad (31)$$

We claim that $b_i z^{-i} + b_{2n-i} z^{-2n+i}$ always contains the factor $1 - \alpha z^{-2}$. To see this, substituting in $z^{-2} = \alpha^{-1}$ to (31), we can observe that $\left[\left(\alpha^{i-n} - 1\right) + \left(\alpha^{-i+n} - 1\right) z^{-2n+2i}\right] = \left[\left(\alpha^{i-n} - 1\right) + \left(\alpha^{-i+n} - 1\right)\alpha^{i-n}\right] = 0$, which proves that $1 - \alpha z^{-2}$ is a common factor of $b_i z^{-i} + b_{2n-i} z^{-2n+i}$. Since $b_n = 0$, $B_Q(z^{-1})$ in (30) thus contains the common factor $1 - \alpha z^{-2}$.